

Semi-Lagrangian Flux Scheme for the Solution of the Aerosol Condensation/Evaporation Equation

Khoi Nguyen and Donald Dabdub

Department of Mechanical and Aerospace Engineering, University of California Irvine, Irvine, California

A new method is developed to solve the condensation equation as it relates to air quality models using both semi-Lagrangian and Lagrangian fluxes to increase resolution and perform accurately under stringent conditions that occur in the atmosphere. The new method, partitioned flux integrated semi-Lagrangian method (PFISLM), can be used with lower-order interpolators and produces highly accurate results. PFISLM is positive definite, peak retentive, mass conservative, and suppresses oscillations. Research indicates that the differences between PFISLM and traditional flux integrated semi-Lagrangian methods as proposed by Bott (1989) and Emde (1991) are significant when solving the aerosol condensation/evaporation equation. PFISLM is created to handle specific difficulties associated with the time and space discretization of the aerosol operator in air quality models.

INTRODUCTION

Air quality models (AQMs) that include aerosol dynamics often employ the continuous distribution approach (Pilinis 1990) to represent aerosols undergoing evaporation and condensation. The fundamental equation governing the condensation process for an internally mixed aerosol is derived in Pilinis (1990). The equation is given as

$$\frac{\partial p_i}{\partial t} = H_i p - \frac{1}{3} \frac{\partial H p_i}{\partial \mu},$$
 [1]

where p_i , H_i , μ , $p = \sum_{i}^{n} p_i$, and $H = \sum_{i}^{n} H_i$ are the mass distribution of species i, mass transfer rate of species i, log of the diameter of the particle, total concentrations, and total mass transfer rates, respectively, with n being the number of aerosol compounds.

Received 10 April 2000; accepted 5 June 2001.

This project was funded in part with federal funds from the National Science Foundation under CAREER grant ATM-9985025 and the Earth System Science thrust area of the National Partnership for Advanced Computational Infrastructure.

Address correspondence to Donald Dabdub, Department of Mechanical and Aerospace Engineering, University of California Irvine, Irvine, CA 92697-3975. E-mail: ddabdub@uci.edu

Typically, Equation (1) is solved by means of operator splitting (Yanenko 1971) into 2 parts: the growth,

$$\frac{\partial p_i}{\partial t} = H_i p, \qquad [2]$$

and the redistribution,

$$\frac{\partial p_i}{\partial t} = -\frac{1}{3} \frac{\partial H p_i}{\partial \mu}.$$
 [3]

The growth term is solved by an exact integration (Wexler et al. 1994). The redistribution term is an advection-like equation, where $\frac{H}{3}$ can be thought of as wind velocity. Hence the redistribution has been computed traditionally by an advection solver. A study of different types of advection solvers used in the solution of the redistribution term is presented in Dhaniyala and Wexler (1996). They recommend a modified Bott solver (1989) to compute the redistribution efficiently and accurately. Further comparisons among advection solvers for the condensation equation are presented in Yang et al. (1999). The redistribution equation is particularly difficult due to its hyperbolic nature. Oscillations and diffusion cause erroneous waves and underprediction of peaks (Oran and Boris 1987). Furthermore, many schemes used to solve the advection equation fail to conserve mass and are not positive definite.

Important Characteristics of AQMs

AQMs that include aerosols typically consume most of the computational time solving the aerosol thermodynamics operator (Meng et al. 1998). The thermodynamics module computes the mass transfer rate that is used in the dynamics of condensation and evaporation of aerosols. To better understand the computational profile of the aerosol operator, the California Institute of Technology (CIT) airshed model (Harley et al. 1993) is used as a host model. The CIT model is a three-dimensional aerosol model used to analyze aerosol dynamics in the South Coast Air Basin of California. The model has 47 gas species and 19 aerosol species distributed into 8 bins. The computational cost of the aerosol operator inhibits the use of a large number

of bins to discretize the continuous distribution. With 8 bins, the CIT model requires 5 days to simulate a 24 h episode on a typical workstation. The number of bins discretized in other aerosol models varies between 2 and 12. With a low number of bins, it is crucial to use an accurate solver to resolve the aerosol distribution.

Three-dimensional AQMs use operator splitting to solve the general aerosol dynamic equation. Typically the splitting is performed as follows:

$$L\{c\} = T_x \left(\frac{\Delta t}{2}\right) T_y \left(\frac{\Delta t}{2}\right) T_{ch-z}(\Delta t) T_{aero}(\Delta t) T_y \left(\frac{\Delta t}{2}\right) T_x \left(\frac{\Delta t}{2}\right),$$
[4]

with T_x , T_y , T_{ch-z} , T_{aero} , and c representing the transport in x, transport in y, z-transport and chemistry, aerosol operator, and species concentration, respectively. The aerosol operator, T_{aero} , solves the condensation equation in the order of 70 times. That is, within each major aerosol operator time-step Δt , the operator in turn takes approximately 70 growth and redistribution time steps. During these growth and redistribution computations the mass distribution of the aerosols is not affected by any other processes inside T_{aero} . After the growth and redistribution are computed, the thermodynamic equilibrium is recomputed by SCAPE2 (Kim et al. 1993; Meng et al. 1998). With these facts in mind, a new solver is created to address the low bin numbers and to take advantage of the large number of condensation computations.

ALGORITHM DESCRIPTION

Redistribution: Semi-Lagrangian Flux Integrated Methods Utilizing Langragian Fluxes

The redistribution operator given in Equation (3) is an advective equation that has been widely studied (Rood 1987; Chock 1991; Dabdub and Seinfeld 1994). Flux integrated semi-Lagrangian (FISL) methods have been used successfully to solve these advective problems (Bott 1989; Emde 1991; Walcek and Aleksic 1998). FISL methods are attractive due to mass conservation and positive definiteness properties. In particular, the CIT airshed model uses the modified Bott solver to compute the redistribution part. In traditional FISL methods, the flux between bins, F, is computed as the mass that evacuates interface I as denoted in Figure 1. The computation of the evacuated mass is performed via an integration of the mass distribution inside each flux partition:

$$F_I = \int_{\mu_1}^{\mu_2} p_i(\mu) \, d\mu.$$
 [5]

Depending on how the mass distribution is interpolated, a variety of different schemes arise. For example, Bott uses Lagrange polynomials, Emde uses quadratic splines, and Walcek uses sharpened linear interpolators. New mass distributions are

Semi-Lagrangian Position of Interface I

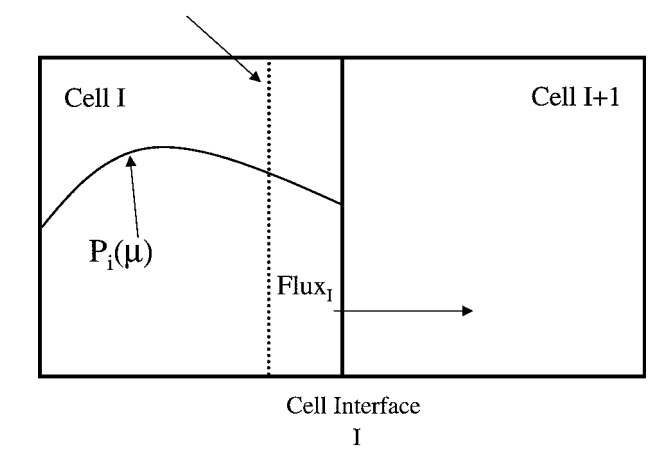


Figure 1. Traditional FISL methods use the primitive function of the mass distribution to evaluate the flux leaving cell interface I. This flux is added to the mass of cell II by a means of averaging over the entire cell.

computed by applying a mass balance:

$$p_i(t + \Delta t) = \frac{F_I - F_{I-1}}{\Delta \mu}.$$
 [6]

Because flux methods are derived from a mass balance, stable flux schemes are always mass conservative. Positive definiteness is maintained either by flux limiting or by monotonic constraints (Laprise 1995; Bott 1989).

The new scheme is a superset of FISL methods. In the new scheme, partitioned flux integrated semi-Lagrangian method (PFISLM), both semi-Lagrangian fluxes and Lagrangian positions are used to resolve the discretization. A graphical representation of the new scheme is shown in Figure 2. A typical semi-Lagrangian flux is the mass that is contained from the semi-Lagrangian position of the cell interface (μ_1) to the cell interface (μ_2) . The evacuated semi-Lagrangian flux enters the partition defined by the cell interface (μ_2) and the Lagrangian position (μ_3) . This area from (μ_2) to (μ_3) is known as a partition. Since the total mass in cell I + 1 is known by (6), the distribution inside each cell is further resolved. Namely, the mass occupied by the first partition, μ_2 to μ_3 , is $p^1 = F_I$; the mass occupied by the second partition, μ_3 to μ_4 , is $p^2 = p_i(t)$; and the mass occupied by the third partition, μ_4 to μ_5 , is $p^3 = F_{II}$. In the next time step, the mass distribution inside cell I + 1 is interpolated more accurately because more information is available to describe the mass partitioning inside the cell due to the Lagrangian partitioning. Depending on the mass transfer rate, each cell can have up to 3 partitions. Figure 3 shows the possible scenarios of this method. PFISLM is always a superset of FISL methods because in FISL methods the mass occupied by p^1 , p^2 , and p^3 are lumped together. This lumping tends to cause greater diffusion.

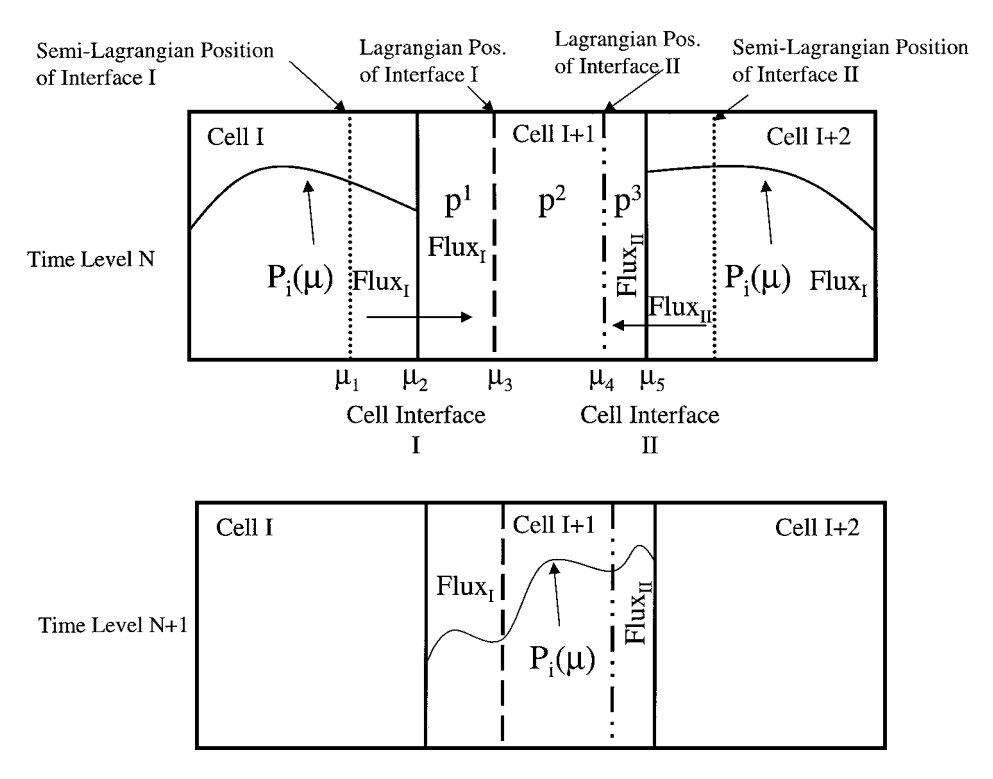
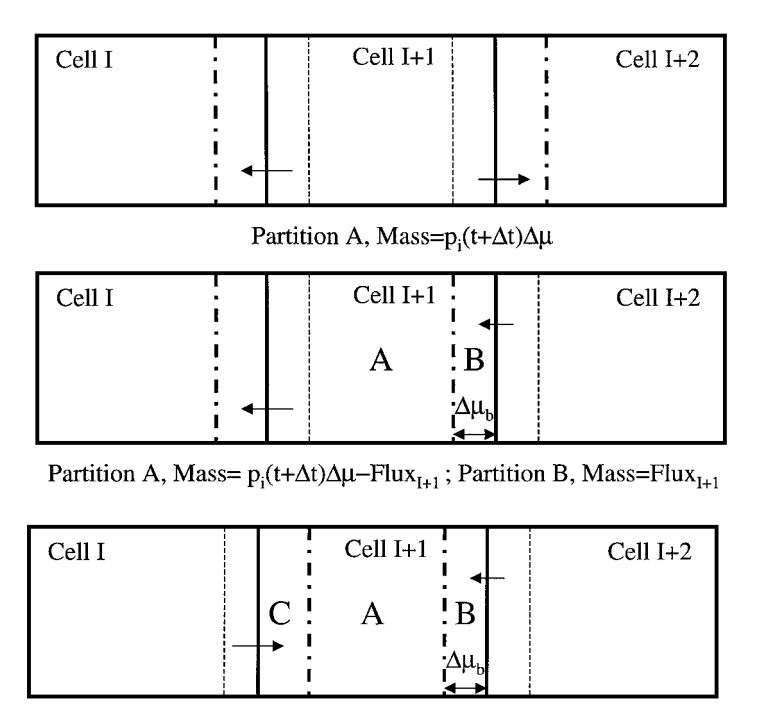


Figure 2. The new method, PFISLM, uses both the semi-Lagrangian and the Lagrangian position of cell interfaces in its computation. The flux leaving cell interface I is not averaged into cell I+1, but is recorded into the partition defined from μ_2 and μ_3 . These partitions permit accurate interpolation as indicated in time level N+1.



Partition A, Mass= $p_i(t+\Delta t)\Delta \mu$ -Flux_{I+1}-Flux_I; Partition B, Mass=Flux_{I+1}; Partition C, Mass=Flux_I

Figure 3. Three possible scenarios that could arise from PFISLM. The first scenario occurs when the fluxes are leaving cell I + 1. The second occurs when one flux is entering and the other is exiting cell I + 1. The final possibility is when both fluxes enter cell I + 1. These possibilities lead to either 1, 2, or 3 partitions to better resolve each cell.

PFISLM has 2 subtle points that must be addressed. First, the information stored in each partition is used upon the next iteration within a single aerosol operation. The mass in each partition is unchanged by other physical processes during the T_{aero} operation, as stated in the previous section. The redistribution and growth are computed numerous times and thus the information in each partition is used effectively. Second, because of the relatively low number of available bins, this method provides greater resolution by having additional information from each partition.

Growth

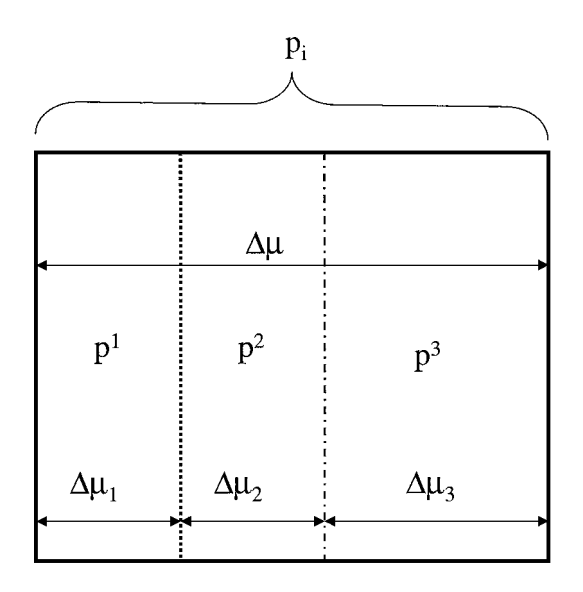
The growth term given in Equation (2) is computed from a mass balance and the growth law. In Figure 4, a sample cell with 3 different partitions is shown. The growth is computed for the entire cell and is distributed to the enclosed partitions accordingly. The growth for the entire cell is found by a direct integration of the growth equations,

$$\frac{\partial p_i}{\partial t} = H_i p, \tag{7}$$

$$\frac{\partial p}{\partial t} = Hp. ag{8}$$

The solution to those 2 simultaneous equations is given as

$$p_i(t + \Delta t, \mu) = p_i(t, \mu) + \frac{H_i}{H} p(t, \mu) [e^{H\Delta t} - 1].$$
 [9]



$$p_i \Delta \mu = p^1 \Delta \mu_1 + p^2 \Delta \mu_2 + p^3 \Delta \mu_3$$

Figure 4. Schematic of a representative case with 3 partitions in the cell. PFISLM is designed to be mass conservative, thus the total mass occupied by the whole cell is equal to the sum of the masses in each partition. The growth is computed for the entire cell and allocated to each partition according to a mass conservation argument.

The mass increase or decrease in each partition is computed by solving a simple set of equations that represents mass conservation, the solution to the growth equation, and the contribution of the cell growth from each partition in accordance to its relative mass to the entire cell. That set of equations is given as

$$p_i \Delta \mu = p^1 \Delta \mu_1 + p^2 \Delta \mu_2 + p^3 \Delta \mu_3,$$
 [10]

$$growth = \frac{H_i}{H} p(t, \mu) \left[e^{H \Delta t} - 1 \right],$$
 [11]

$$massgrowth_j = massgrowth \frac{mass_j}{mass}.$$
 [12]

Here the *massgrowth* is the growth of the mass in the entire cell, *growth* is the growth of concentration in the entire cell, *mass_j* is the mass occupied by partition j, *massgrowth_j* is the growth of the mass in partition j, p_i is the concentration in the entire cell, and p^j is the concentration in partition j. Substituting $massgrowth_j = growth_j \Delta \mu_j$, $massgrowth = growth \Delta \mu$, and $mass_j = p^j \Delta \mu_j$ into Equation (12), the solution to the growth term in each partition is obtained by

$$growth_j = growth \frac{p^j}{p_i}.$$
 [13]

Other algorithms can be used to distribute the growth in a cell to its partition as long as they are mass conservative. For example, algorithms that exploit the variations of the condensation rate and species concentration within each partition can be used. The method developed here is the simplest to implement by assuming no spatial variations for the concentration and condensation rate within each partition.

DESCRIPTION OF NUMERICAL TESTS

Tests are developed to represent situations encountered in the atmosphere. In particular, the number of bins used in tests resembles those used in air quality models. Other comparisons have been presented in the scientific literature using 30 bins, which is excessive with the computational requirements of AQMs. Here, tests are performed with the more reasonable amount of 12 bins. Tests should also represent the conditions of actual models in regard to the rate of condensation and the number of actual condensation computations. As described subsequently, the condensation equation in AQMs requires accurate solvers if these tests are developed to have similar conditions to actual AQMs.

Three schemes are compared: a Bott solver with a fourth-order Lagrange polynomial, which has been considered superior to various other solvers by Dhaniyala and Wexler (1996); a PFISLM with a linear interpolation; and a PFISLM with quadratic interpolation. The quadratic interpolation is analogous to the one used by Emde (1991). The new solver is independent of interpolators; a linear and a quadratic interpolator are used due to their ease of implementation. Any other interpolator could be used so long as the interpolation represents the primitive function of the mass distribution. This condition is met when the integral

of the interpolator over each partition is equal to the mass occupied by each partition. As with FISL methods that yield a host of new schemes with different interpolators, PFISLMs also yield a host of new and more highly resolved schemes.

Test I-A: Condensation and Evaporation of Cosine Hills. Test I-A is an ideal case with constant condensation rates. Using 12 bins and 20 species, different cosine hills are condensed and evaporated back and forth until the number of required iterations is met. The test is performed for 4 Courant numbers, $\frac{H}{3\Delta x}\Delta t$, of 0.1, 0.2, 0.4, 0.5. Higher Courant numbers need not be tested since they should not be used in AQMs. The number of iterations that the solver must perform in this test is set to 200, a stringent but common number of iterations that the aerosol operators use to compute condensation in AQMs. For example, it is found that condensation gains mass and redistributes relatively quickly, thus more mass is introduced into the bins, which require recomputation of the mass transfer coefficients. This cycle is repeated until the aerosol operator time step is met. The recomputation of mass transfer coefficients is the primary reason why larger Courant numbers should not be used: the cell should not evacuate more than half of its contents before the recomputations of the mass transfer rate is performed. Mathematically, Test I-A uses the following initial conditions:

$$p_i(\mu) = \begin{cases} \frac{i}{20} \left(1 + \cos \left[\frac{\mu - 5}{4} \right] \right) & \text{if } |\mu - 5| \le 4, \\ 0 & \text{otherwise,} \end{cases}$$

with the mass transfer rate defined for corresponding Courant numbers with i = 1...20.

$$H_i = H_j = \frac{0.3}{20}, \frac{0.6}{20}, \frac{1.2}{20}, \frac{1.5}{20}.$$
 [14]

A schematic of this test case is shown in Figure 5. The cosine hills are condensed until the base of the cosine hill reaches the boundary, evaporated back at the same rate to the initial conditions, and then condensed again. The condensation—evaporation cycle is repeated until 200 iterations are met. The final solution is expected to equal the initial condition. By condensing and evaporating back and forth, the test is able to gauge schemes at a high number of iterations without reaching the boundaries and without growing unbounded due to the exponentiation of the growth term. This test case is more stringent than that presented in Dhaniyala and Wexler (1996), since it requires more iterations, and represents AQMs accurately. In brief, Test I-A gauges the peak retentive properties of solvers under a large number of iterations.

Test I-B: Condensation and Evaporation of Step Concentrations. This test is similar to Test I-A except for the initial conditions, which are now step functions of height 1.0 for the submicron particles and have no concentrations for particles larger than 1.0 micron. The submicron particles condense into the larger bins and then evaporate back to the initial conditions. The number of iterations are the same as in Test I-A. Test I-B

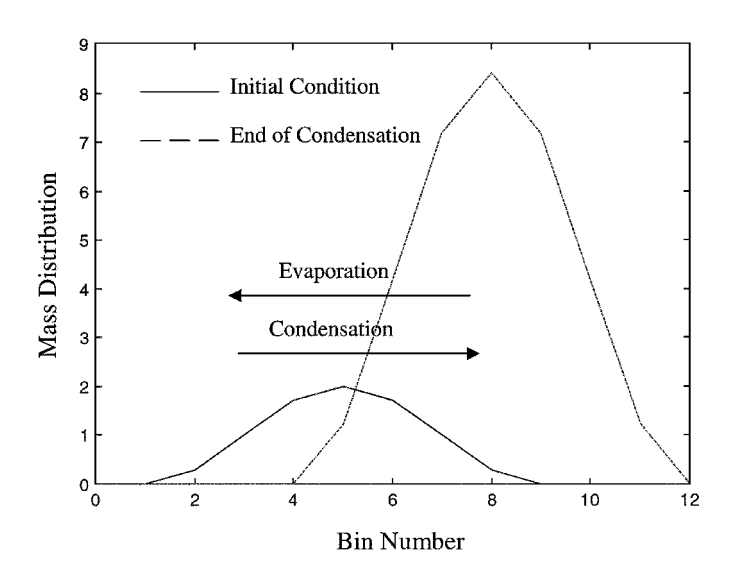


Figure 5. Schematic of Test I, where cosine hills are undergoing condensation and then evaporation. Each cosine hill condenses until the base of the cosine hill reaches the boundary. At that point, the cosine hill evaporates back to the initial condition. This procedure is repeated for 200 iterations.

is demanding due to the high frequency Fourier modes in the step functions; transport of those modes with many iterations provides a stringent test for stability and accuracy.

Test II: Hazy Conditions. Test II is described by Seigneur et al. (1986) and represents hazy conditions in urban areas. Sulfuric condensation rates are $5.5 \, \mu \text{m}^3 \text{cm}^{-3}$ per 12 h. The growth law is given by Fuchs and Sutugin (1971) as

$$\frac{dv}{dt} = \frac{4\pi r D}{1 + \left(\frac{1.333\text{Kn} + 0.71}{1 + \text{Kn}}\right)\text{Kn}} v_m P,$$
 [15]

where D is the diffusion coefficient, Kn is the Knudsen number, P is the ambient vapor pressure, r is the radius, and v_m is the molecular volume of the condensing vapor. Hazy conditions in urban areas represent a stringent test due to its larger mass transfer rate. The performance of various solvers for Test II are presented by Zhang and Seigneur (1999). Test II gauges the performance of solvers under realistic growth rates, and the solvers' ability to suppress oscillations.

Test III: Practical Application. The final test is a full implementation in the CIT airshed model (Harley et al. 1993). The CIT model includes advection, diffusion, chemistry, deposition, and emissions. The episode simulates August 27 and 28, 1987, for the South Coast Air Basin of California. The domain is irregular and has 5 layers in the vertical direction with 994 grid points in each layer. The domain could be tightly fitted inside a rectangular domain of 50×27 grid points. The spacing between each grid point in a layer represents 5000 m. There are 47 species in the gas phase and 19 species in the aerosol phase using 8 fixed bins in the simulation. The aerosol thermodynamics is computed using SCAPE2 (Kim et al. 1993; Meng et al.

1998). Test III compares the performance and accuracy of the modified Bott solver (Dhaniyala and Wexler 1996) and PFISLM implemented in the CIT model to solve the aerosol condensation/evaporation equation.

RESULTS

The following performance indices are evaluated to measure the relative accuracy among the algorithms:

$$MD = \frac{\sum_{x,y} c(x, y, t)^{2}}{\sum_{x,y} c(x, y, 0)^{2}},$$
 [16]

$$MA = \frac{\text{Max} [c(x, y, t)]}{100},$$
 [17]

$$ME = \frac{\text{Max} |c(x, y, t) - c_{exact}(x, y, t)|}{100},$$
 [18]

where *MD*, *MA*, and *ME* are the mass distribution ratio, maximum ratio, and maximum error ratio, respectively. Mass conservation and minimum ratio are not supplied since all 3 schemes tested are mass conservative and positive definite.

Figure 6a shows the results of Test I-A for a Courant number of 0.4. Because the test condenses and evaporates the cosine hill back and forth, the exact solution is the initial cosine hill. In Figure 6a, the Bott solver displays large diffusive errors. PFISLM implemented with a linear and quadratic interpolator shows more accurate results. Table 1 displays the performance of the schemes for various Courant numbers. The Bott solver

Table 1
Performance of the 3 schemes with Test I-A for 4 different
Courant numbers

	Bott (%)	PFISLM w/linear (%)	PFISLM w/quadratic (%)
CFL = 0.1			
Error ratio	19.8	3.7	6.6
Mass distribution ratio	81	97	93
Maximum ratio	84	99	95
CFL = 0.2			
Error ratio	28.4	8.7	7.8
Mass distribution ratio	74	93	92
Maximum ratio	76	95	95
CFL = 0.4			
Error ratio	34.8	7.7	2.9
Mass distribution ratio	70	92	98
Maximum ratio	71	94	99
CFL = 0.5			
Error ratio	35.3	0.0	0.0
Mass distribution ratio	70	100	100
Maximum ratio	71	100	100

Table 2
Performance of the 3 schemes with Test I-B for 4 different
Courant numbers

Courant numbers				
	Bott (%)	PFISLM w/linear (%)	PFISLM w/quadratic (%)	
CFL = 0.1				
Error ratio	23.6	11.0	14.8	
Mass distribution ratio	93	94	94	
Maximum ratio	117	104	107	
CFL = 0.2				
Error ratio	27.7	14.0	17.0	
Mass distribution ratio	93	93	94	
Maximum ratio	120	105	110	
CFL = 0.4				
Error ratio	30.8	14.1	13.2	
Mass distribution ratio	93	94	96	
Maximum ratio	124	106	105	
CFL = 0.5				
Error ratio	31.7	0.0	0.0	
Mass distribution ratio	94	100	100	
Maximum ratio	125	100	100	

has problems with lower Courant numbers, while the PFISLM performs relatively well even though it uses low-order interpolators. It is important to note that at a Courant number of 0.5, the PFISLM is perfect. In fact, the method has 3 Courant number regions where it provides exact performance. Namely, at Courant numbers near 0, 0.5, and 1, the method has increased accuracies. This is due to the fact that the new method takes advantage of both semi-Lagrangian and Lagrangian positions to increase its performance throughout the Courant number range.

Table 2 presents the performances of the various schemes for Test I-B. After the cycles of condensation and evaporation, the PFISLM with linear interpolation provided the most accurate solution for this test. The primary reason for the better performance of the linear interpolation is due to the high frequencies associated with a step function. With lower order interoplation much of the noise from higher frequencies can be reduced. Figure 6b gauges the ability of the various schemes to maintain the shape of the inital conditions. This test is particularly stringent due to the high frequency inherent in the step function and the number of condensation/evaporation cycles. The best time step to use for an accurate solution is for the Courant Number of $\frac{1}{2}$, where both interpolations with the PFISLM schemes did not propagate any errors. The best time performance of the 3 schemes are from the Bott solver. Given that the Bott solver took 1.0 time units, PFISLM with linear interoplation took 1.6 time units and PFISLM with quadratic interoplation took 1.9 time units. However, due to the high accuracy of the PFISLM methods, larger time steps can be taken without loss to accuracy, as Tables 1 and 2 present. Furthermore, the results of Test III, shown later, also

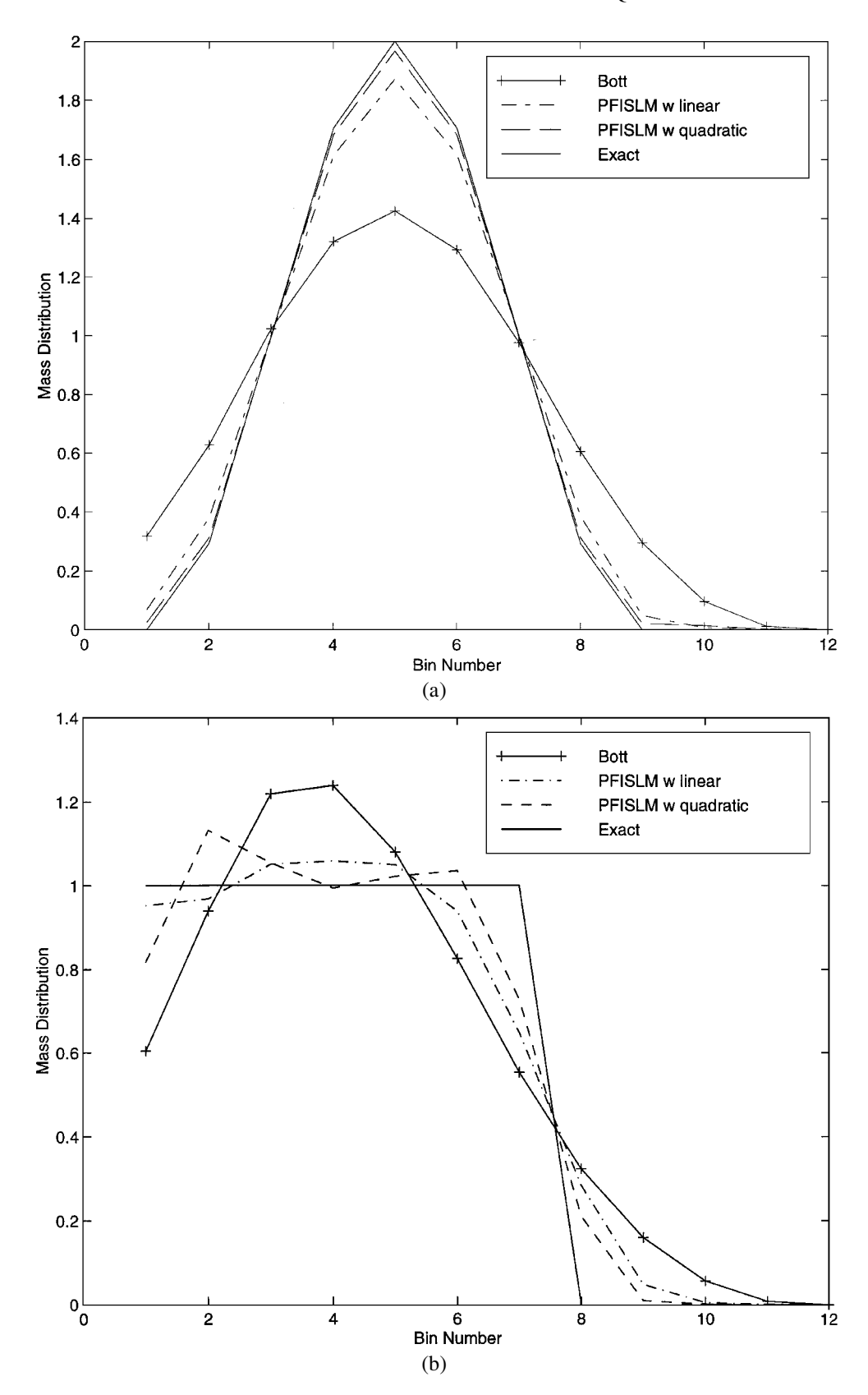


Figure 6. (a) The results of Test I-A show that the Bott solver is diffusive, while the PFISLM with linear and quadratic interpolators preserve the peaks within 10%. (b) The results of Test I-B show results similar to Test I-A in Figure 6a. The stringent initial conditions are particularly difficult due to the inherent high frequencies of the step functions.

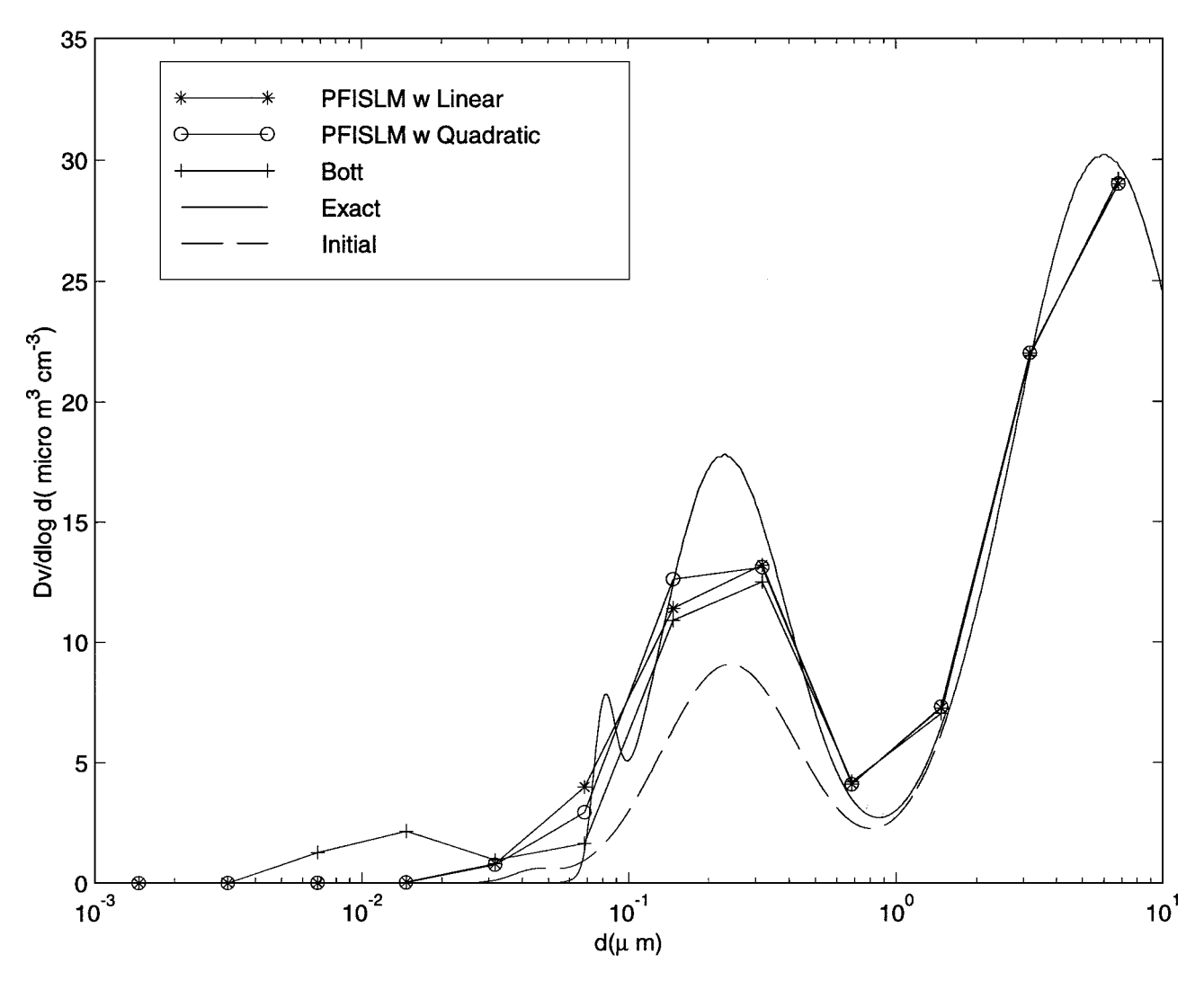


Figure 7. Test II gauges the performance of the solvers with respect to oscillation suppression. The Bott solver has an erroneous growth in the peak in bin number 4. This peak is due to oscillations and amplification of this oscillation by the growth law. This erroneous peak consumes much of the available gas for the peak in bin 7 to grow where it is supposed to be. PFISLM with linear and quadratic interpolators is able to represent the peak at bin 7 within 4%.

support the use of larger time steps in three-dimensional airshed models.

Figure 7 shows the resulting mass distribution of Test II. In this case the initial condition condenses to the higher final solution. The "exact" solution is computed using 500 bins and taking small time steps. The Bott solver behaves erratically at lower bins with an erroneous peak near 0.01 μ m. The new solver with the quadratic interpolator predicts the concentration between 0.1 μ m and 2.15 μ m with an average absolute normalized error of 8.1%. PFISLM and Bott have errors of 9.5% and 11.1%, respectively. The erroneous peak near 0.01 μ m from the Bott solver is due to small oscillations that occur at lower bins. The oscillations are amplified by an exponential growth law for lower bins, as indicated by Equation (9). The problem is then compounded since the erroneous peak consumes much of the

available gas. With the available gas nearly depleted, the second peak near 1.0 μm is not able to grow to where the exact solution is. If the oscillations in the Bott solver are suppressed using artificial filters, Bott performs better (results not shown). PFISLM suppresses erroneous growth due to its increased resolution provided by the partitioning. For example, suppose a bin cell has 2 equally spaced partitions, 1 with 0 mass distribution and the other with unity mass distribution. Typical FISL methods would average the 2 partitions, resulting in a cell mass distribution of 0.5. Thus the growth law causes the cell to grow throughout. With PFISLM, the first partition does not grow since a 0 mass distribution is recognized. Only the second partition grows as dictated by the growth law. The results are not averaged but kept in each partition. This is the primary reason that PFISLM is better suited to handle growth.

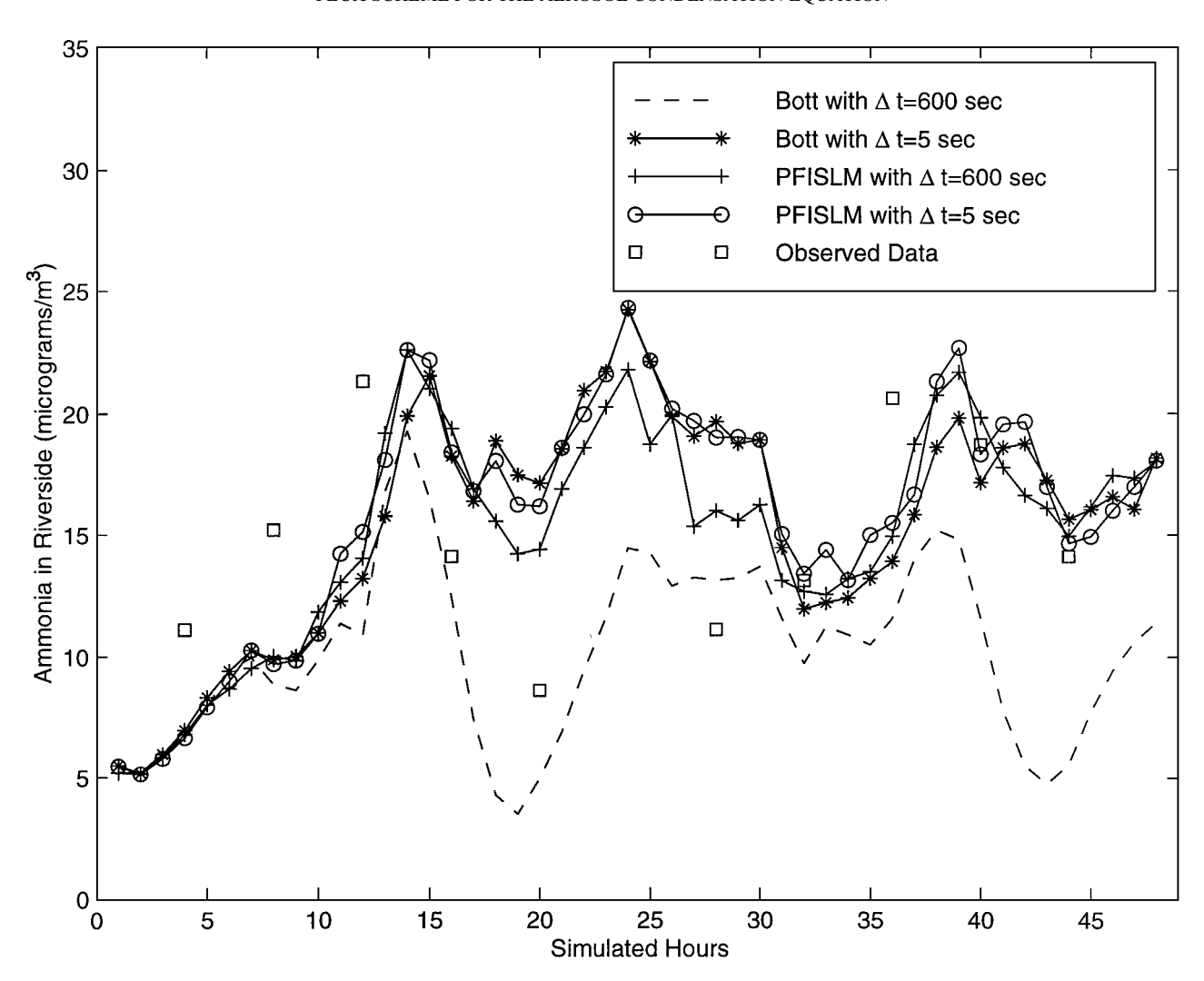


Figure 8. Results from Test III in Riverside for ammonia indicate a similarity between Bott and PFISLM when maximum time steps are smaller at 5 s for ammonia $PM_{2.5}$. At the efficient maximum time step of 600 s, which is currently implemented, the Bott solver deviates considerably from the 5 s simulations. PFISLM with 600 s agrees within 10% of the 5 s simulations.

Some results to Test Case III are presented in Figures 8–10. The city of Riverside is chosen due to its high particulate matter (PM) concentration of nitrates and ammonia. The city of Los Angeles is also chosen to represent a simulation of an ammonia poor condition. The CIT airshed model uses a maximum permitted time step of 600 s for solving the condensation/evaporation equation. To better ascertain the accuracy of PFISLM and Bott, a maximum time step of 5 s is set for both Bott and PFISLM. The results in Figure 8 indicate that with a maximum time step of 5 s, both PFISLM and Bott produce similar results. However, with the maximum time step of 600 s, only PFISLM agrees with the 5 s simulations within 10%. The similarity of PFISLM with 600 s and that of PFISLM and Bott with 5 s is also observed for ammonia at Riverside. Figure 9 presents the predicted concentrations of nitrate PM_{2.5} in Riverside. Similar behavoir is exhibited between nitrate and ammonia $PM_{2.5}$ due to their combined path of formation from ammonium nitrate. In both species,

ammonia and nitrate, the observed data is better matched with the Bott solver for August 27. However, for August 28, ammonia and nitrate are better predicted by the PFISLM solvers and the Bott solver using a stringent maximum time step of 5 s. The Bott solver with 600 s differs from the 5 s simulations by up to 70%. At lower bin numbers, this difference is even greater. The differences between the new solver and the Bott solver are due to the diffusive nature of the Bott solver for many iterations. These results confirm conclusions obtained from Tests I-A and I-B, which resemble the stringent nature of the host model's conditions. The simulated results from Los Angeles in Figure 10 show similar patterns as those in Figures 8 and 9. The PFISLMs and the Bott method using the maximum time increment of 5 s are similar. The Bott solver using the original maximum permitted time step of 600 s underpredicted the ammonia concentrations in Los Angeles. The critical issue is that all the PFISLM schemes and the Bott with

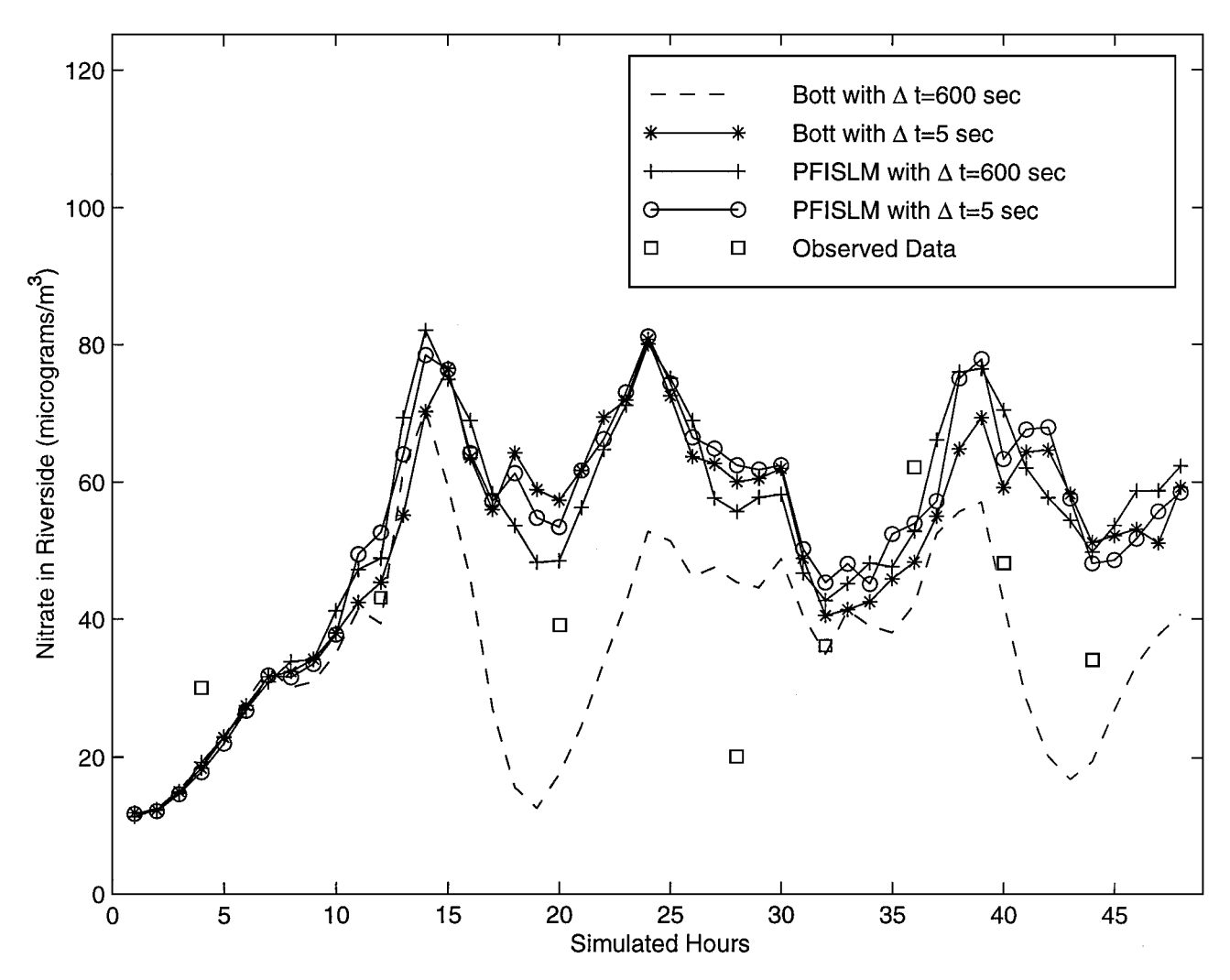


Figure 9. Results from Test III in Riverside for nitrate indicate a similarity between the Bott solver with the maximum time step of 5 s and the PFISLM with 5 and 600 s maximum time steps. The Bott solver using the maximum time steps of 600 s is substantially different from the other schemes. The similarity between ammonia $PM_{2.5}$ in Figure 8 and nitrate $PM_{2.5}$ predictions is due to their shared path of formation by ammonium nitrate.

5 s time steps are similar, while the Bott with 600 s is substantially different. This is observed for all major species and locations throughout the modeling domain. The performance times for the Bott solver and PFISLM with a quadratic interpolation using a 32 node parallel machine are similar. For the case with the maximum time step of 5 s, the episode using the Bott solver is 1.15 times slower than PFISLM. In the episode with the maximum time step of 600 s, the Bott solver is 1.12 times slower than the PFISLM. On average, each day of simulation with the 600 s maximum time step requires 5 h on a Pentium III 933 MHz.

Test III shows that in order to achieve convergence in real applications Bott requires small (and expensive) time steps to advance the solution accurately. Due to the similarity between the PFISLM and Bott solver using the maximum 5 s and the

PFISLM using 600 s, the PFISLM using 600 s provides an advantageous reduction in computational time.

CONCLUSIONS

The condensation/evaporation equation plays a vital role in the prediction of PM in AQMs. The inherent computational cost of the aerosol operator inhibits the use of a large number of bins. The rapid transport between the gas and the aerosol phase components makes the aerosol dynamics equation particularly difficult to compute accurately. The redistribution part of the aerosol operator resembles the wind advection in AQMs. However, the redistribution of aerosols is more challenging than wind advection due to the smaller inherent time scales of the aerosol operator and limited grid points. A new approach to solving

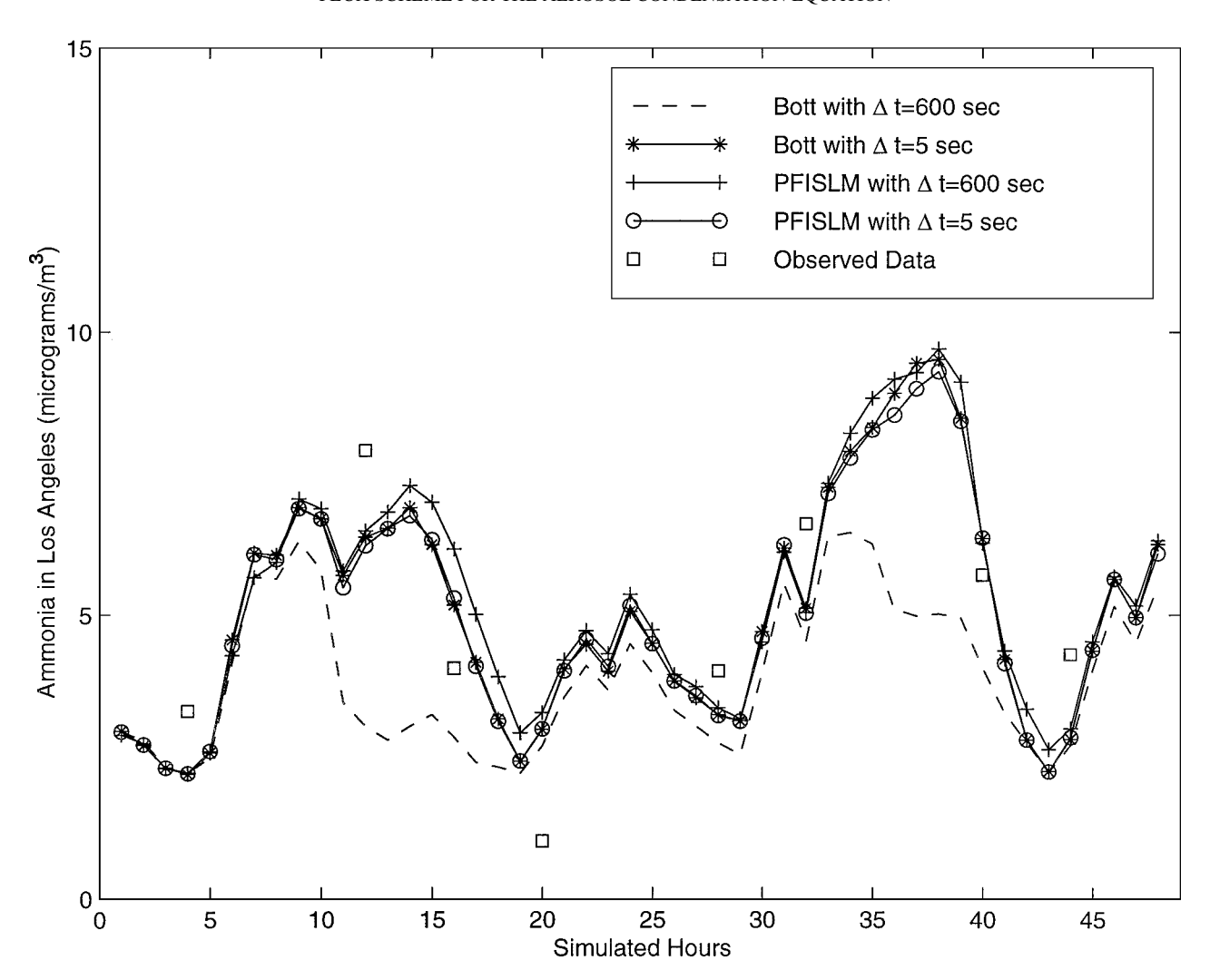


Figure 10. Results from Test III in Los Angeles for ammonia indicate similar behavior of the various schemes as that of Riverside. The Bott solver using the maximum permitted time step of 600 s does not predict results that are congruent to those of the other schemes. However, the PFISLM method using the maximum time step of 600 s can adequately reproduce the performance as that with smaller time steps.

the condensation equation is developed to handle these difficult characteristics of the aerosol operator. The new method is mass conservative, positive definite, peak retentive, and suppresses oscillations. The approach is a superset of flux integrated semi-Lagrangian methods using both semi-Lagrangian and Lagrangian fluxes. It effectively increases the resolution of the bins by keeping information about the partitions inside each bin. This increased resolution permits accurate representation of the actual dynamics of aerosols, especially with a limited number of bins.

This paper presents new tests better suited to stringent conditions. Research has shown that the Bott solver is inaccurate under conditions of current AQMs. The difference in results between the new solver and the Bott solver is reflected in both test cases and in the CIT airshed model. Differences of up to 70% are computed due to the diffusive nature of the Bott solver. The

largest differences in the CIT airshed model occur at lower bins and in the afternoon hours.

REFERENCES

Bott, A. (1989). A Positive Definite Advection Scheme Obtained by Nonlinear Renormalization of the Advective Fluxes, *Mon. Wea. Rev.* 117:1006–1015.

Chock, D. P. (1991). A Comparison of Numerical Methods for Solving the Advection Equation—III, Atmos. Environ. 25A:853–871.

Dadbub, D., and Seinfeld, J. H. (1994). Numerical Advection Schemes used in Air Quality Models–Sequential and Parallel Implementation, *Atmos. Environ*. 28:3369–3385.

Dhaniyala, S., and Wexler, A. (1996). Numerical Schemes to Model Condensation and Evaporation of Aerosols, *Atmos. Environ.* 30:919–928.

Emde, K. (1991). Solving Conservation Laws with Parabolic and Cubic Splines, Mon. Wea. Rev. 120:482–492.

Fuchs, N. A., and Sutugin, A. G. (1971). High Dispersed Aerosols, in *Topics in Current Aerosol Research*, G. M. Hidy and J. R. Brock, eds., Ann Arbor Science Publishers, Ann Arbor, 1–60.

- Harley, R. A., Russell, A. G., McRae, G. J., Cass, G. R., and Seinfeld, J. H. (1993).
 Photochemical Modeling of the Southern California Air Quality Study, Environ. Sci. Technol. 27:378–388.
- Kim, Y. P., Seinfeld, J. H., and Sexena, P. (1993). Atmospheric Gas-Aerosol Equilibrium I, Thermodynamic Model, *Environ. Sci. Technol.* 19:157–181.
- Laprise, J. P., and Plante, A. (1995). A Class of Semi-Lagrangian Integrated-Mass (SLIM) Numerical Transport Algorithms, Amer. Met. Soc. 123:553–565.
- Meng, Z., Dabdub, D., and Seinfeld, J. H. (1998). Size-Resolved and Chemically Resolved Model of Atmospheric Aerosol Dynamics, J. Geophys. Res. 103:3419–3435.
- Oran, E. S., and Boris, J. P. (1987). *Numerical Simulation of Reactive Flow*, Elsevier, New York.
- Pilinis, C. (1990). Derivation and Numerical Solution of the Species Mass Distribution Equations for Multicomponent Particulate Systems, *Atmos. Environ*. 24:1923–1928.

- Rood, R. B. (1987). Numerical Advection Algorithms and Their Role in Atmospheric Transport and Chemistry Models, Rev. Geophys. 24:71–100.
- Seigneur, C., Hudischewskyi, A. B., Seinfeld, J. H., Whitby, K. T., Witby, E. R., Brock, J. R., and Barnes, H. M. (1986). Simulation of Aerosol Dynamics: A Comparative Review of Mathematical Models, *Aerosol Sci. Technol.* 5:205–222.
- Walcek, C. J., and Aleksic, N. M. (1998). A Simple but Accurate Mass Conservative, Peak-Preserving, Mixing Ratio Bounded Advection Algorithm with FORTRAN Code, Atmos. Environ. 32:3863–3880.
- Wexler, A. S., Lurmann, F. W., and Seinfeld, J. H. (1994). Modeling Urban and Regional Aerosols—I. Model Development, *Atmos. Environ.* 28(3):531–546.
 Yanenko, N. N. (1971). *The Method of Fractional Steps*, Springer, New York.
- Yang, Z., Seigneur, C., Seinfeld, J., Jacobson, M., and Binkowski, F. (1999). Simulation of Aerosol Dynamics: A Comparative Review of Algorithms used in Air Quality Models, *Aerosol Sci. Technol.* 31:487–514.